Appl. Phys. A 54, 244–250 (1992)

Applied Physics A Solids and Surfaces

Resolution of Photothermal Tomographic Imaging of Subsurface Defects in Metals with Ray Optic Reconstruction

M. Munidasa, A. Mandelis, and C. Ferguson

Photothermal and Optoelectronic Diagnostics Laboratory, Ontario Laser and Lightwave Research Centre and Department of Mechanical Engineering, University of Toronto, Toronto, Ont. Canada, M5S 1A4

Received 23 July 1991/Accepted 21 November 1991

Abstract. A capacitive photopyroelectric tomographic technique to obtain photothermal images of cross-sections with subsurface defects of opaque solid samples is reported. Unlike the two-dimensional "projection" images obtained by conventional photothermal detection methods, a tomographic scanning sequence has been used for cross-sectional imaging of subsurface features. Ray-like propagation of thermal waves is assumed in reconstructing the images. Resolution of these tomographic images with multiple features is investigated. Sensitivity of this reconstruction method to the size and shape of a single subsurface defect is also discussed.

PACS: 07.68, 81.70, 77.70

Photothermal imaging has emerged as a useful technique for nondestructive evaluation (NDE) of subsurface features in opaque solids [1, 2] complementary to conventional techniques such as ultrasonic and X-ray inspection. Due to the heavily damped nature of thermal waves, this method is most suitable in detecting near-surface defects ranging from few micrometers to several millimeters. In thermal wave imaging a beam of energy (laser or electron beam), modulated at a certain frequency is focused and scanned across the sample surface. The resulting periodic heat flow in the material is a diffusive process, producing a periodic temperature distribution which is called a "thermal wave". These waves will reflect and scatter from features beneath the surface which have different thermal characteristics from their surroundings. The signal detected due to these processes taking place at subsurface boundaries is a function of the relative position of the heat source and the detector. Also the amount of energy absorbed at the surface is determined by the surface properties which will vary from point to point on the surface. Several different detection methods [2] have been used to detect these thermal waves. Each method has its own advantages and disadvantages.

Recently, a pyroelectric instrumentation [3, 4] using polyvinylidene fluoride (PVDF) films electroded on one side only, and a remote metal tip capable of sampling the local thermal wave field value in the back of the sample [5] has been developed. This permits spatially resolved scans of this field. A photothermal image obtained using this method has been shown to be better resolved spatially than the same image obtained from a spatially integrated detection method (PVDF film electroded on both sides) [2, 6]. Since both modulated heating source and detector pin are localized, and can be scanned independently, it is also possible to perform a limited angle tomographic scan using this instrument. Conventional photothermal images obtained from this and other photothermal methods are two-dimensional "projections" of subsurface features obtained in a two dimensional raster scan without regard to the actual depth position of scatterers. Although, work has been done in obtaining depth-resolved information on subsurface features using an equivalent experimental technique [7] and Mirage effect scanning [8], these techniques have not been tomographically implemented. The frequency dependent penetration depth of thermal waves has also been utilized for depth profiling of layered [9] and continuously inhomogeneous [10] samples. A method which utilizes the spectral cross-correlation technique to obtain the thermal impulse response has been succesfully used [11] to image different layers of materials. A time-domain (transient) thermal pulse depth profiling technique akin to that utilized by Uejima et al. [11] has been used very recently and has been called "dynamic thermal tomography" [12]. Subsequently, this method combined with an IR camera has been used to form thermal wave slice images, which were called "tomograms" [13, 14].

Numerically searching the temporal peak of the reflected thermal waves from subsurface features on a pixel-by-pixel basis, these authors obtained a sequence of images of time (or depth) slices. This method is capable of revealing defects through subsurface slice imaging, only if the subsurface defects are not overlapping in the direction perpendicular to

the surface (the direction of heat propagation), and are embedded in an otherwise homogeneous material. This is so because, the temporal peak of the reflected thermal waves depends on the (generally locally varying) thermal diffusivity of the material through which the thermal wave diffuses. Therefore, the image carries spatially convoluted information from the entire path which has been thermally traversed until the observation instant. Due to the fact that no spatial deconvolution (demultiplexing and reconstruction) takes place with "dynamic thermal tomography" and its imaging applications, it is not a proper tomographic methodology, but rather a very special usage of the word "tomography". It is well known that spatial deconvolution is an essential aspect of the various tomographic techniques [15] (e.g., non-diffracting sources: X-ray, photon and positron emission; and diffracting sources: ultrasonic, microwave, optical etc.). Entirely analogous experimental procedures, based on the transient thermal response and the construction of thermal depth images from the intensity and the delay characteristics of the signal at a given instant, have been reported without a "tomographic" label [16]: Features appearing at a particular instant after the pulse corresponded to defects at a specific depth [13, 16]. The very special definition of the "dynamic thermal tomography" coined by Vavilov [12] and its derivative techniques has been actually discussed by the author himself, who has claimed that "it is impossible to use the viewing of solids under different space angles as in X-ray tomography, but the only solution is to investigate the time behavior of the temperature field". This is, indeed, the case with Vavilov's and related techniques, and earlier on with Uejima et al.'s methods [11]. As an immediate consequence of their not being true tomographies, these spatially non-demultiplexing methodologies cannot be successful in resolving subsurface (defect) structures at different depths (z), which otherwise overlap in the (x, y) coordinates. It is important to point out that, in this context, the scanning technique presented by Busse and Renk [7] is consistent with, and can lead to, true thermal wave tomography as it satisfies the criterion of the ability to spatially demultiplex the signal. On the other hand, the Mirage effect scanning [8] can yield a two-dimensional image upon demultiplexing in the (x, y) surface plane, which still remains a projection image with thermal-diffusion length limited, integrated depth information. Therefore, it is only partially tomographic, related to backprojection tomography.

In a recent paper [17] we reported the preliminary work performed towards reconstructing an actual spatially demultiplexed thermal wave tomographic image using the pyroelectric detection instrumentation reported earlier [5]. Ray-like propagation of thermal waves was assumed [18] in order to demonstrate the possibility of thermal wave tomography. In [17] we followed the conventional nondiffracting tomographic scanning method as in X-ray and positron emission tomographies and the solid is viewed under different space angles, exactly what was claimed by Vavilov [12] to be impossible for thermal waves. Two aluminum samples of thickness 2 mm with a subsurface hole of diameter 1 mm and 0.5 mm, respectively, were used in that experiment. It was observed that the position of the smaller hole is more accurately reproduced in this method of reconstruction. It was also observed that increasing modulation frequency tends to move the position of the hole towards the front surface from its actual position. This has been partially eliminated by averaging the two reconstructed images obtained from the data collected from both sides of the sample. In this paper we will continue to use the same reconstruction method to image cross-sections with multiple features to study the resolution of these images.

1 Experimental Method

A complete description of the instrumentation used can be found elsewhere [3–5, 17]. This involves a pyrolelectric thin film (with only one electroded surface) attached to the back surface of the sample where the electroded surface is in contact with the sample. For spatially resolved measurements the back surface electrode of the film is replaced with a metal pin of diameter 0.5 mm, so that the local ac electric field which is proportional to the ac temperature field at the back surface of the sample generated by the modulated laser beam (1.0 W Nd:YAG (1.06 μm) laser focused onto the metal sample, beam diameter: 20 μm) may be sampled. The signal is synchronously detected by a lock-in amplifier. The sample and the pin are mounted on separate micrometer stages driven by stepping motors. Scans across cross-sections to be imaged were performed as shown in Fig. 1. For each laser position, data were collected at several pin positions (27 for the data presented in this paper) along a straight line PQ (Fig. 1b), which defines the cross-sectional plane ($PQRS$ of Fig. 1a) to be imaged.

Three circular aluminum samples of thickness 2 mm and diameter 15 mm with different subsurface defects were used in this experiment. Figure 2a shows the top view and a typ-

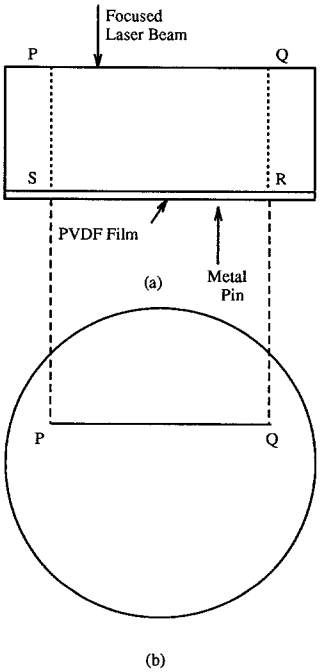

Fig. 1. a Sample cross-section with the film attached to the back. Cross-section to be imaged is $PQRS$ where the laser beam is scanned between P and Q, and the pin is scanned between S and R. **b** Top view of the sample surface showing the scan line PQ

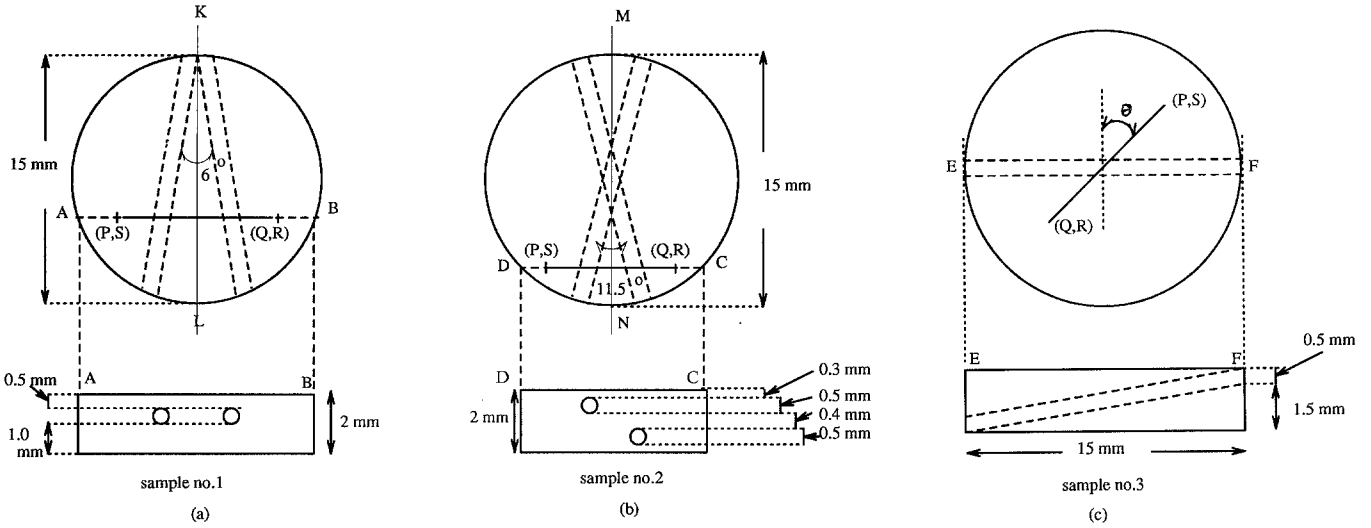

Fig. 2a–c. The top view and a typical cross-section (shown at the bottom of each sample) of three circular aluminum samples of thickness 2 mm and diameter 15 mm with different fabricated subsurface defects. The points P, Q, R, and S in all three figures represent the same points in Fig. 1. **a** Sample no. 1 with two subsurface holes drilled at an angel parallel to the sample surface, **b** sample no. 2 with two holes drilled at an angle crossed at the center of the sample and located at two different depths, and **c** sample no. 3 with a slanted hole along a diameter of the sample, are shown by dashed lines. See text for detailed dimensions

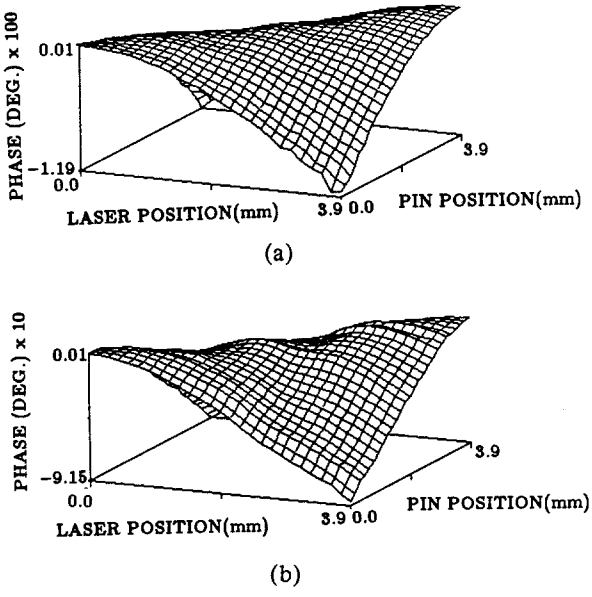

Fig. 3a, b. A plot of phase data vs laser/pin position obtained at a modulation frequency of 20 Hz from tomographic scans along a line as shown in Fig. 2a, b, of **a** sample no. 1 and **b** sample no. 2

ical cross-section of sample no. 1 to be imaged, with two subsurface holes of diameter 0.5 mm drilled at an angle of 6° to each other parallel to the sample surface. The axes of both holes are at a depth of 0.75 mm from one surface. Sample no. 2 has two holes of diameter 0.5 mm at a top-view angle of 11.5° crossed at the center of the sample and located at two different depths as shown in Fig. 2b. The axes of the holes are located at a depth of 0.55 mm and 1.45 mm, respectively, from one surface. To study how our tomographic reconstruction method reflects the change in size and shape of a subsurface feature, a third sample with a 0.5 mm diameter slanted hole (sample no. 3, Fig. 2c) was used. Scans were made (modulation frequency of 20 Hz) along a line PQ (Fig. 2c) through the center of the sample (where P and Q are the first and the last laser positions, respectively and S and R are the two end points of the pin scan at the back) for three different angles θ, so that the shape and size of the hole cross-section were different in each scan.

Figure 3a shows a plot of phase data (laser/pin-position vs phase of the signal) obtained at a modulation frequency of 20 Hz from a tomographic scan along a line 2.8 mm away from the edge K of sample no. 1 (Fig. 2a), perpendicular to the diameter KL. Laserposition P and pinposition S in Fig. 1 (also in Fig. 2a) refers to the coordinate (0 mm, 0 mm) in Fig. 3a. A similar set of data with a modulation frequency of 20 Hz obtained from a tomographic scan along a line 3.65 mm away from the center of sample no. 2 (Fig. 2b), perpendicular to the diameter MN is shown in Fig. 3b. Since the photothermal amplitude data are dominated by the inhomogeneities in the surface reflectance [17, 19], only phase data are used in this work.

2 Reconstruction Method

A reconstruction algorithm based on ray-like propagation of thermal waves in one-dimension:

$$T(x,t) = T_0 \exp(-x/\mu)\cos(\omega t - x/\mu) \tag{1}$$

is used [17]. Here, T is the ac temperature at a distance x from the heated surface, T_0 is the temperature input at the heated surface, μ is the thermal diffusion length, and ω is the modulation angular frequency. Equation (1) is used to calculate the average value of the thermal diffusivity, α, given by

$$\alpha = \frac{\omega}{2}\mu^2 \tag{2}$$

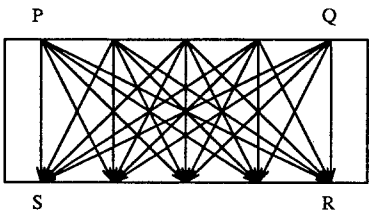

Fig. 4. The cross-section $PQRS$ to be imaged is shown with rays joining laser positions and pin positions for a five laser/pin position scan

along the lines joining the heated spot and the pin from the corresponding data. Each cross-section to be imaged is divided into rectangular pixels. By averaging over each line, values of α for each individual pixel are calculated. This method is equivalent to the algebraic reconstruction technique (ART) used in X-ray tomography [20]. Figure 4 shows a cross-section with rays joining laser positions and pin positions for a five laser-pin position scan. The value of α (used as the imaged quantity) for each pixel is weighed by the distance a ray travels across that particular pixel. A normalized value of $\alpha = 2\,\mathrm{cm^2\,s^{-1}}$ has been used as the reference which corresponds to aluminum with no defects. Limitations of this reconstruction method have been discussed in [17] under identical experimental conditions and will not be repeated here.

3 Tomographic Reconstructions and Discussion

The reconstructed image of the data in Fig. 3a ($\omega/2\pi = 20\,\mathrm{Hz}$, $\mu = 1.2\,\mathrm{mm}$, where $\alpha = 0.9\,\mathrm{cm^2/s}$) is shown as a contour plot in Fig. 5a. In this and other figures to follow, background with artifacts [17] of the image due to edge effects of reconstruction has been suppressed to enhance the known features (computer-aided image enhancement). In all the tomographic images presented here, actual positions of the hole cross-sections are indicated by circles. In Fig. 5a, the centers of the holes are 0.75 mm deep and they are 0.78 mm apart. Figure 5b shows the reconstructed image of the same cross-section obtained from the data collected at the same modulation frequency by flipping the sample, so that the depth of the holes is now 1.25 mm. In this image the two holes are no longer resolved showing the deterioration of the resolution with increasing depth. In the reconstructed image (Fig. 5c) of the same cross-section of Fig. 5b, but from 80 Hz ($\mu = 0.6\,\mathrm{mm}$) data the two (deep) holes are resolved, showing the expected increase in resolution with frequency. These observations are related to the broadening of the images due to the diffusive nature of thermal waves. Increasing source-to-scatterer distance (increasing depth) and increasing thermal diffusion length (decreasing frequency) broaden the image width leading to lower spatial resolution and poor delineation of subsurface thermal boundaries. This type of behavior has been ovserved and extensively studied in conventional thermal wave imaging [21–23]. In Fig. 5c the positions of the holes are not accurately reproduced. The same cross-section obtained at 80 Hz by averaging the two images at 0° and 180° (flipped) positions gave improved hole positioning compared to Fig. 5c, as reported earlier [15]. This double-side scanning requirement turns out to be very important for accurate reconstructions in thermal wave tomography, at least in its ray-optic approximation.

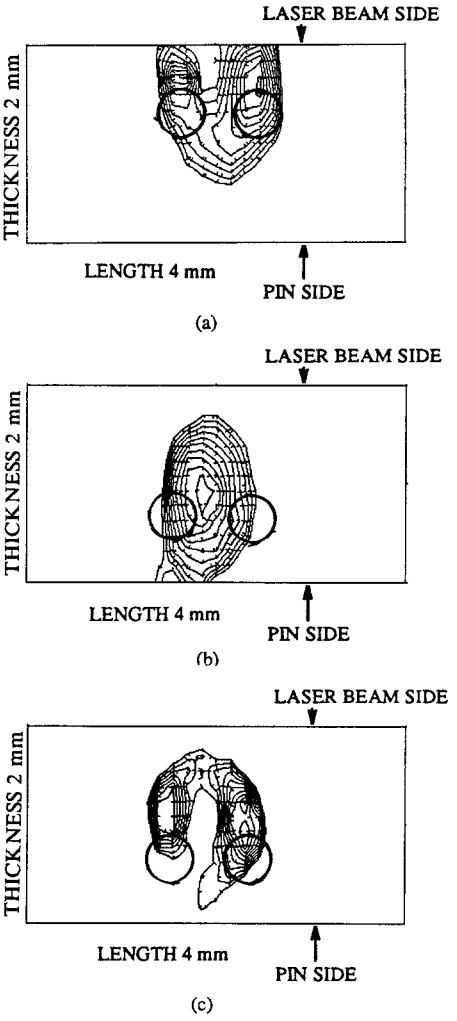

Fig. 5. a A contour plot of the reconstructed image from the data in Fig. 3a. In this and the other figures to follow, actual positions of the hole cross-sections are indicated by thick circles. The centers of the holes are 0.75 mm deep and they are 0.78 mm apart. **b** A contour plot of the same cross-section as in **a** obtained by 180° rotation of the sample. Here the holes are 1.25 mm deep. **c** Image of the same cross-section as in **b** reconstructed from the data obtained at a modulation frequency of 80 Hz

Figure 6a shows the single-side tomographic reconstruction of a cross-section in sample no. 2, 3.65 mm away from the center of the sample, perpendicular to MN (Fig. 2), obtained from data taken at 90 Hz. In this cross-section the center of the shallower hole is 0.55 mm (compared to the hole depth of 0.75 mm in sample no. 1) below the surface and has moved to the surface in the reconstructed image. Figure 6a also shows that the contrast of the shallower hole is much greater than the deeper hole, making the two holes almost unresolvable. Figure 6b shows the same cross-section at 20 Hz (data shown in Fig. 3b). Here the two holes are clearly resolved. At 90 Hz the thermal diffusion length of aluminum is about 0.56 mm making the shallower hole stronger scat-

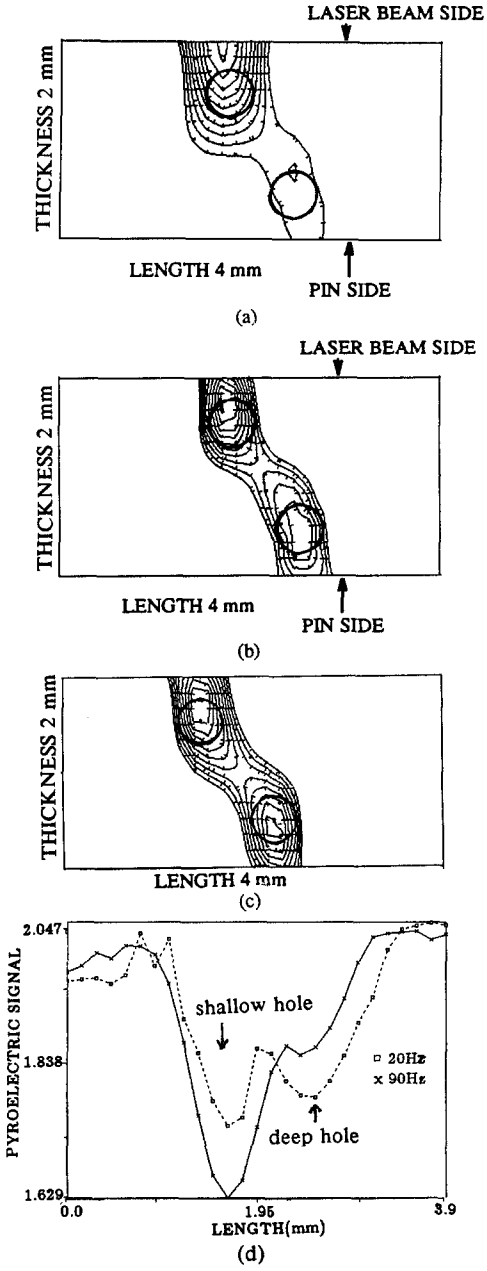

Fig. 6. a The reconstructed image from the data obtained at a modulation frequency of 90 Hz from a tomographic scan along a line as shown in Fig. 2b, top view, 3.65 mm away from the center of sample no. 2. The centers of the holes are 0.55 mm and 1.45 mm deep and they are separated horizontally by 0.72 mm. **b** Same cross-section as in **a** reconstructed from the data obtained at 20 Hz. **c** Image of the same cross-section as in **b** obtained at 20 Hz by averaging the two images at 0° and 180° rotation of the sample. **d** Conventional photothermal line scan along the same line as in **b** obtained by scanning the laser and the pin together with the pin just below the laser at 20 Hz (squares) and 90 Hz (crosses)

terer of thermal waves. The deeper hole is well outside one diffusion length. At 20 Hz when the diffusion length is 1.2 mm both holes are within in reach of one diffusion length, so that scattering from both holes is comparable. Figure 6c shows the cross-section of Fig. 6b obtained at 20 Hz by averaging the two images at 0° and 180° positions. The

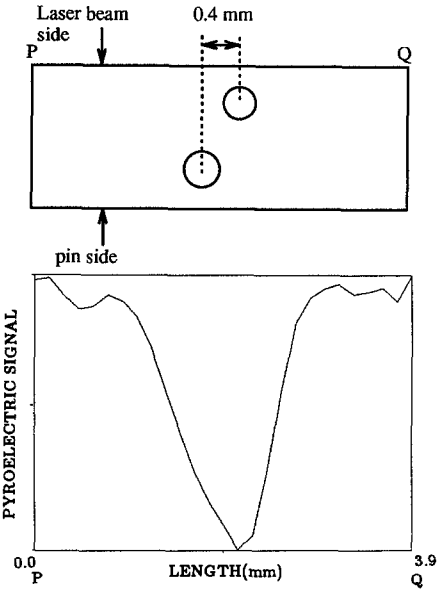

Fig. 7. Conventional photothermal line scan along the line PQ (sample no. 2) as shown in the cross-section, obtained by scanning the laser and the pin together, with the pin just below the laser, at 20 Hz. The two holes are horizontally separated by 0.4 mm

double scan has produced a more accurate positioning of the center of each hole than the single scan [15], and has yielded equal intensity contours from each hole, as expected from the identical construction and geometry of the two holes. Figure 6d shows the conventional photothermal line scans of the same cross-section obtained at two different frequencies by scanning the laser and the pin together with the pin just below the laser spot. This also shows improved spatial resolution at lower frequency.

When the two holes partially overlap in the vertical direction or even when the horizontal separation between the two holes is zero, conventional two-dimensional (projectional) scanning will not be able to separate the two. Figure 7 shows such a line scan where the hole centers are separated by 0.4 mm. The reconstructed tomographic image of the same cross-section at 20 Hz obtained from the single-scan data of the sample, is shown in Fig. 8a. This barely shows the presence of the deeper hole. When the images obtained from both sides are averaged, the positions of both holes are clearly separated and accurately placed (Fig. 8b). Although the holes almost overlap vertically, the shortest separation between the two hole centers (0.98 mm) is still larger than the horizontal separation (0,78 mm) in Fig. 5b. Viewing the cross-section from different space angles (tomographic scanning) has enabled us to resolve these subsurface features, a characteristic of this spatial demultiplexing method, not feasible with Vavilov's "dynamic thermal tomography" [12] and derivative imaging methods [11, 13, 14, 16]. Comparison between Fig. 5b and Fig. 8b seems to indicate that thermal-wave tomographic resolution is higher for in-depth superposed features than for lateral features coexisting at the same depth, when both geometries are probed at low frequencies.

Reconstructed single-scan images of different cross-sections of the single slanted hole (Fig. 2c) at $\theta = 0°$, 65°

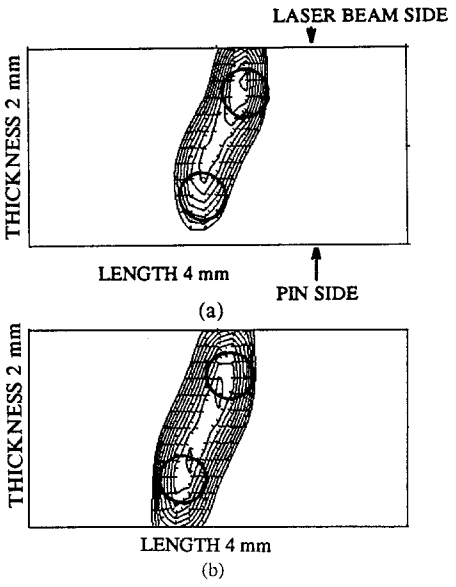

Fig. 8. a Reconstructed tomographic image of the cross-section shown in Fig. 7 obtain from single-side scan data at 20 Hz. **b** Same cross-section as in a obtained by averaging the two images from both sides of the sample (0° position and 180° rotation)

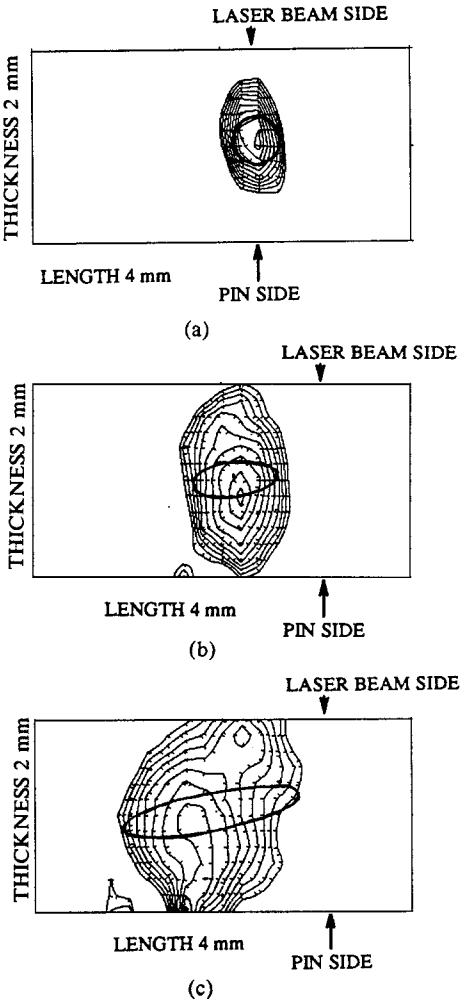

Fig. 9a–c. Reconstructed single-scan (0° rotation only) images of different cross-sections of the single slanted hole (sample no. 3, Fig. 2c) along the line (P, S)–(Q, R) in Fig. 2c for $\theta =$ (**a**) 0, (**b**) 65, and (**c**) 80 degrees

and 80° are shown in Fig. 9a–c respectively, all drawn to the same scale. Although the change in size of the hole cross-section is reflected clearly in these tomograms, the change in shape is distorted. This distortion is most apparent in Fig. 9c and is partially due to the lack of adequate numbers of scan laser-pin lines to allow substantial thermal wave propagation outside the hole (i.e. in surrounding metal), as the feature size has increased to occupy most of the scanned space. Scanning farther away than shown in Fig. 9 has resulted in very poor signals due to the large laser-pin distances involved, and cannot be utilized as higher spatial frequencies to improve the delineation of large subsurface features, at least in the rayoptic approximation. This effect must be considered together with trends in all rayoptic reconstructed thermal-wave tomograms to appear elongated in the direction perpendicular to the cross-sectional scan. It is this elongation/distortion which is responsible for the inaccurate positioning of single-scan tomograms, such as Figs. 5a, c, 6a, b, and 8a. This distortion may be due to the significant loss if information from other scattering angles outside the pin diameter at each beam-pin position. This information scatter loss is due to the highly diffractive nature of thermal wave propagation and cannot be accounted for in the rayoptic approximation. Proper field inversion based on the recently proven Laplace Diffraction Theorem [24] is likely necessary in order to enhance the fidelity of the image reconstruction. The lack of inversion symmetry in diffractive thermal wave propagation is partially compensated by the double scan procedure, which averages line integral features lying closer to, and farther than, each surface with signals obtained by interchanging source and detector. This procedure tends to equalize the relative weights of deep lying features when the sample is flipped over (180° rotation) with those lying close to the front, laserbeam exposed surface. It is expected that a 90° rotation can adequately fill the Laplace wavenumber (spatial frequency) space of the tomogram [24], so that for rotations at 0, 90, 180, and 270° will produce well delineated sub-surface images with optimal degree of reconstruction fidelity. With our present instrumentation and sample geometries the 90° and 270° rotations are not practical.

4 Conclusions

In this report we have examined the spatial resolution of cross-sectional images obtained by photothermal tomographic scanning. Results from sample no. 1 with two holes at the same depth show that the spatial resolution increases with increasing modulation frequency and with decreasing defect depth, similar to conventional photothermal scanned imaging. When the two defects are at different depths, however, the capability of depth resolution in tomographic imaging makes the two defects resolved even if they overlap in the vertical direction, a unique feature of the spatial demultiplexing nature of thermal wave tomography. Due to the

heavily damped nature of thermal waves, with the assumption of ray-like propagation, better results are obtained by double scanning following at 180° sample rotation and when the defects are within one thermal diffusion length. Low-frequency scanning, however, results in a loss of resolution. To overcome these difficulties, a reconstruction method which takes into account the diffractive [24–26] and heavily damped nature of thermal waves is required. Results from sample no. 3 suggest that to obtain the correct shape of the defect, another set of data obtained from directions orthogonal to the present set is needed.

Acknowledgements. The authors gratefully acknowledge the support of the Natural Sciences and Engineering Research Council of Canada (NSERC) towards the realization of this work.

References

1. R.L. Thomas, L.D. Favro, P.K, Kuo: Can. J. Phys. **64**, 1234–1237 (1986)
2. M. Munidasa, A. Mandelis: *Progress in Photoacoustic and Photothermal Science and Technology,* ed. by A. Mandelis, Vol. 1 (Elsevier, New York 1992) pp. 299–367
3. M. Mieszkowski, K.F. Leung, A Mandelis: Rev. Sci. Instrum. **60**, 306–316 (1989)
4. A. Mandelis, M. Mieszkowski: Thermal wave sub-surface defect imaging and tomography apparatus, U.S. Patent 4,950,897 (1990)
5. M. Mieszkowski, A. Mandelis: J. Opt. Soc. Am. A **7**, 552–557 (1990)
6. C. Ferguson: B. A. Sc. Thesis, Dept. of Mechanical Engineering, University of Toronto (1991)
7. G. Busse, K.F. Renk: Appl. Phys. Lett. **42**, 366–368 (1983)
8. D. Fournier, F. Lepoutre, A.C. Boccara: J. Phys. (Paris) C **6–44**, Suppl. 10, 479–482 (1983)
9. J. Opsal, A. Rosencwaig: J. Appl. Phys. **53**, 4240–4246 (1982)
10. A. Mandelis, E. Schoubs, S.B. Peralta, J. Thoen: J. Appl. Phys. **70**, 1771–1777 (1991)
11. A. Uejima, F. Itoga, Y. Sugitani: Anal. Sci **2**, 113–117 (1986)
12. V.P. Vavilov: SPIE 1313, Thermosense XII, 178–182 (1990)
13. L.D. Favro, T. Ahmed, D. Crowther, H.J. Jin, P.K. Kuo, R.L. Thomas, X. Wang: SPIE **1467,** Thermosense XIII, 290–294, and 132 (1991)
14. L.D. Favro, H.J. Jin, P.K. Kuo, R.L. Thomas, Y.X. Wang: In Proc. 7th Int'l Topical Meeting on Photoacoustic and Photothermal Phenomena, Doowerth, The Netherlands, August 26–30, 497–498 (1991)
15. A.C. Kak, M. Slaney: Principles of Computerized Tomographic Imaging (IEEE Press, New York 1987)
16. J.-C. Krapez, X. Maldague, P. Cielo: Res. Nondestr. Eval. **3,** 101–124 (1991)
17. M. Munidasa, A. Mandelis: J. Opt. Soc. Am. A **8**, 1851–1858 (1991)
18. J.A. Burt: J. Phys. (Paris) **C6–44,** Suppl. 10, 453–457 (1983)
19. G. Busse: *In Optics in Biomedical Sciences,* ed. by. G. von Bally, P. Greguss, Springer Ser. Opt. Sci. Vol. 31 (Springer, Berlin, Heidelberg 1982) pp. 34–37
20. G.T. Herman, A. Lent, S.W. Rowland: J. Theor. Biol. **42,** 1–32 (1973)
21. L.J. Inglehart, K.R. Grice, L.D. Favro, P.K. Kuo, R.L. Thomas; Appl. Phys. Lett. **43,** 446–448 (1983)
22. F.A. McDonald, G.C. Wetsel, Jr., C.G. Clark: Proc. 1983 Ultrasonic Symposium, ed. by B.R. McAvoy (IEEE, New York 1983) pp. 672–676
23. R.L. Thomas, L.D. Favro, K.R. Grice, L.J. Inglehart, P.K. Kuo, J. Lhota: Proc. 1982 Ultrasonic Symposium, ed. by B. R. McAvoy (IEEE, New York 1982) pp. 586–590
24. A. Mandelis: J. Phys. A: Math. Gen. **24**, 2485–2505 (1991)
25. A. Mandelis, K.F. Leung: J. Opt. Soc. Am. A **8**, 186–200 (1991)
26. A. Mandelis: J. Opt. Soc. Am. A **6** 298–308 (1989)